NASA TECHNICAL NOTE

NASA TN D-4357

NASA TN D-4357

FLUTTER OF BUCKLED, SIMPLY SUPPORTED, RECTANGULAR PANELS AT SUPERSONIC SPEEDS

by Robert W. Fralich and John A. McElman

Langley Research Center
Langley Station, Hampton, Va.

NATIONAL AERONAUTICS AND SPACE ADMINISTRATION • WASHINGTON, D. C. • MARCH 1968

FLUTTER OF BUCKLED, SIMPLY SUPPORTED, RECTANGULAR PANELS AT SUPERSONIC SPEEDS

By Robert W. Fralich and John A. McElman

Langley Research Center
Langley Station, Hampton, Va.

NATIONAL AERONAUTICS AND SPACE ADMINISTRATION

For sale by the Clearinghouse for Federal Scientific and Technical Information
Springfield, Virginia 22151 – CFSTI price $3.00

FLUTTER OF BUCKLED, SIMPLY SUPPORTED, RECTANGULAR PANELS AT SUPERSONIC SPEEDS

By Robert W. Fralich and John A. McElman
Langley Research Center

SUMMARY

A theoretical flutter analysis is presented for buckled, simply supported panels subjected to supersonic flow over one surface. The analysis employs the Von Karman large-deflection plate theory and linearized static aerodynamic strip theory. A Galerkin procedure using four static mode shapes is employed to determine a set of differential equations which is programed on an analog computer. The character of the output of the analog is used to determine the flutter speed. Results are obtained for panels with ratios of length in the streamwise direction to length in the cross-flow direction equal to 1/2 and 1 for three specified in-plane edge-loading conditions. An assessment of effects of cross-flow coupling of the modes is made by comparison of the results with those obtained when cross-flow coupling between the modes is neglected.

INTRODUCTION

Panel flutter has been encountered in the operation of aircraft and missiles and has become an important consideration in the design of structures for such vehicles. The panel flutter problem is influenced by many factors, such as aerodynamic effects, effects of boundary conditions and midplane compressive loads, and length-width ratio. In addition, if the midplane compressive stresses are of sufficient magnitude to cause buckling, the flutter problem is further complicated. These various aspects of the flutter problem are discussed, for example, in references 1 to 10; some of the earlier investigations are listed in reference 1. Reference 1 considers the flutter of buckled, simply supported panels. In reference 1 the mechanism for flutter is shown to be a streamwise coupling between the modes. The purpose of the present analysis is to obtain a more accurate solution to this particular problem by investigating cross-flow coupling between the modes. Cross-flow coupling is a phenomenon which does not occur in the small-deflection flutter analysis of unbuckled, simply supported panels.

The results presented in reference 1 were obtained from a two-mode Galerkin solution, and rigorous analytical methods were used to determine the panel stability. In the present analysis a general Galerkin solution is obtained and the stability of the panel is determined for a four-mode solution by use of an analog computer. Points on the flutter

boundaries have been determined for three in-plane edge-loading conditions for ratios of the length in the streamwise direction to the length in the cross-flow direction equal to 1/2 and 1.

SYMBOLS

$A_0, A_1, B_0, B_1, A_{mn}, B_{mn}$ coefficients in displacement expressions (eqs. (9))

a length of plate in streamwise direction

b width of plate in cross-flow direction

C_{mn} amplitude coefficients for lateral displacement

D flexural rigidity, $\frac{Eh^3}{12(1 - \mu^2)}$

E Young's modulus

F_{mn}, G_{mn}, H_{mn} Fourier coefficients (see eqs. (12))

h plate thickness

M Mach number

M_1, M_2, M_3, M_4
P_1, P_2, P_3, P_4
Q, S, T, J, K, N, H parameters defined in equations (21)

m,n number of half-waves in streamwise and cross-flow directions, respectively

N_x, N_y, N_{xy} midplane stress resultants

$\bar{N}_x, \bar{N}_y, \bar{N}_{xy}$ nondimensional midplane stress resultants; $\frac{N_x a^2}{\pi^2 D}$, $\frac{N_y a^2}{\pi^2 D}$, and $\frac{N_{xy} a^2}{\pi^2 D}$, respectively

P_x, P_y average in-plane edge loads per unit length, positive in compression

$\bar{P}_x, \bar{P}_y$ nondimensional in-plane edge loads per unit length; $\frac{P_x a^2}{\pi^2 D}$ and $\frac{P_y a^2}{\pi^2 D}$, respectively

p,q,r,s	integers
q	dynamic pressure, $\frac{1}{2}\rho V^2$
t	time
u,v	in-plane displacements, positive in x- and y-directions, respectively
$\bar{u},\bar{v}$	nondimensional in-plane displacements, positive in x- and y-directions; $\frac{Eha}{\pi^2 D}u$ and $\frac{Eha^2}{\pi^2 Db}v$, respectively
V	free-stream velocity
w	lateral deflection, positive in z-direction
$\bar{w}$	nondimensional lateral deflection, positive in z-direction, $w\sqrt{\frac{Eh}{D}}$
x,y,z	rectangular Cartesian coordinates (see fig. 1)
$\beta = \sqrt{M^2 - 1}$	
γ	mass density of plate material
δ_{mn}	Kronecker delta, equals 1 if $m = n$, equals 0 if $m \neq n$
λ	speed parameter, $\frac{16qa^3}{3\pi^4\beta D}$
λ_{cr}	flutter speed parameter
μ	Poisson's ratio
$\nu = a/b$	
ξ,η	nondimensional coordinates; x/a and y/a, respectively
ρ	free-stream density of fluid
τ	nondimensional time, $\frac{\pi^2}{a^2}t\sqrt{\frac{D}{\gamma h}}$

When subscripts ξ, η, and τ follow a comma, they indicate partial differentiation with respect to ξ, η, and τ, respectively. Dots over symbols denote derivatives with respect to τ.

STATEMENT OF PROBLEM

The configuration analyzed in this report is the simply supported, flat, rectangular panel shown in figure 1. The panel has a constant thickness h with air flowing over the top surface at a Mach number M. No flow of air beneath the panel is considered. Average in-plane edge loads P_x and P_y per unit length (positive in compression) are specified at the boundaries. No in-plane shearing forces are applied to the plate.

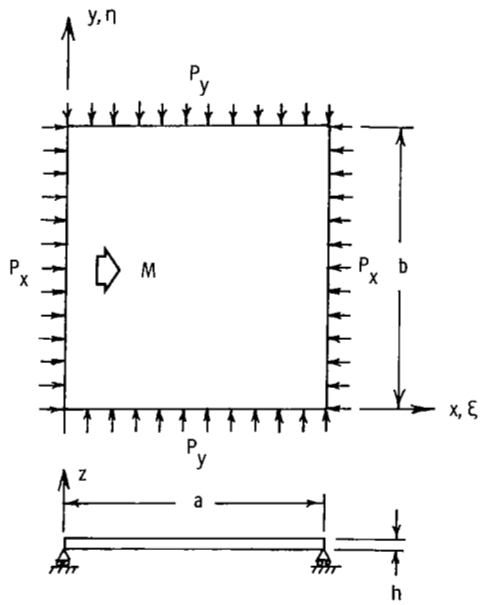

Figure 1.- Rectangular panel and coordinate system.

METHOD OF SOLUTION

The present analysis employs the large-deflection plate theory of Von Karman and linearized static aerodynamic strip theory. This aerodynamic approximation has previously been shown to yield accurate flutter boundaries for Mach numbers greater than about 1.6. The resulting equations are analyzed in the appendix by means of a Galerkin procedure which utilizes the doubly infinite set of static buckling modes. This procedure yields a doubly infinite set of second-order nonlinear ordinary differential equations for the time-dependent amplitude coefficients C_{mn}. These equations can be reduced to those for various approximate analyses that utilize a finite number of static buckling modes. The set of four equations, obtained from an approximate analysis that uses four of the static modes, is analyzed by means of an analog computer in order to find a flutter speed parameter λ_{cr}. The modes considered have amplitude coefficients C_{mn}, where $m = 1$ and 2 and $n = 1$ and 2 are the number of half waves in the streamwise and cross-flow directions, respectively.

In the analog analysis, the character of the time histories of the amplitude coefficients is observed while the initial static buckling condition is altered by gradually increasing the speed parameter λ to a given level. Analog traces which illustrate the method of determining flutter are given in figure 2. For levels of λ below the critical value λ_{cr} (fig. 2(a)), the amplitude coefficients do not build up with time and the motion

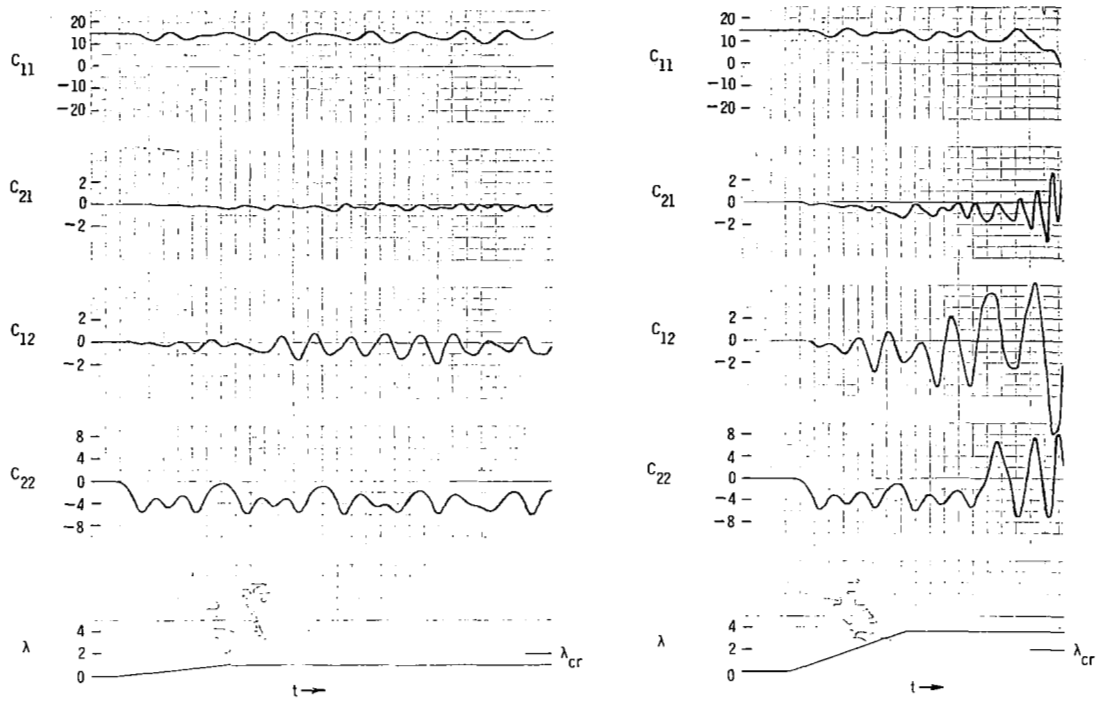

(a) Stable motion. $(\lambda < \lambda_{cr})$

(b) Unstable motion. $(\lambda > \lambda_{cr})$

Figure 2.- Variation of amplitude coefficients with time.

is considered stable. For levels of λ above the critical flutter speed λ_{cr} (fig. 2(b)), the amplitude coefficients show a drastic buildup with time. The character of the motion is observed for different levels of λ until the critical flutter speed parameter λ_{cr} is determined. The value of λ_{cr} for the case illustrated in figures 2(a) and 2(b) is indicated by the tick mark. Values of λ_{cr} are determined for three in-plane loading conditions for two values of a/b, the ratio of length in the streamwise direction to width in the cross-flow direction.

RESULTS AND DISCUSSION

Results for the flutter boundaries obtained from the present analysis are given by the circles in figures 3 to 5. Flutter boundaries $(\lambda = \lambda_{cr})$ are plotted in these figures as a function of in-plane edge loading for a/b of 1/2 and 1. Flutter occurs above these boundaries and stable motion is obtained below the boundaries. Results for specified values of $\bar{P}_x$ with $\bar{P}_y = 0$, for specified $\bar{P}_y$ with $\bar{P}_x = 0$, and for specified $\bar{P}_x = \bar{P}_y$ are shown in figures 3, 4, and 5, respectively. Also shown in these figures are the flutter boundaries presented in reference 1 which were obtained by a rigorous stability analysis using just two modes. The curve labeled $n = 1$ is the flutter

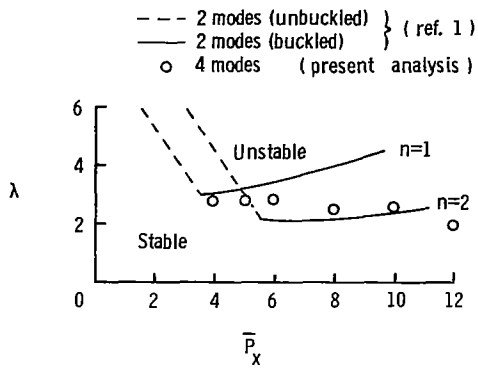

(a) $\nu = 1/2$.

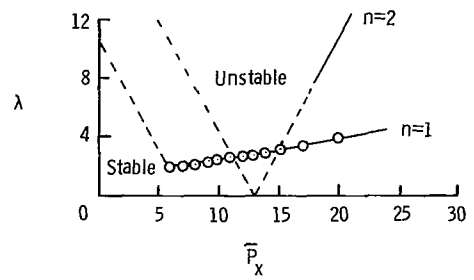

(b) $\nu = 1$.

Figure 3.- Flutter boundaries for panels with streamwise compressive load $\bar{P}_x$. $\bar{P}_y = 0$.

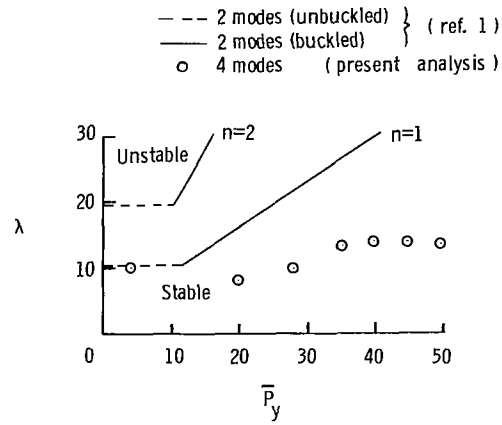

Figure 4.- Flutter boundaries for panels with cross-flow compressive load $\bar{P}_y$. $\bar{P}_x = 0$; $\nu = 1$.

boundary obtained by considering only the C_{11} and C_{21} modes, whereas the one labeled n = 2 utilizes the C_{12} and C_{22} modes.

The results show effects of cross-flow coupling of the modes on the flutter of simply supported, rectangular panels in supersonic flow. Theoretically, this coupling does not exist on the portion of the flutter boundary prior to buckling (the dashed line portions of figs. 3, 4, and 5). One result in the present four-mode analysis was determined in the unbuckled range. (See fig. 4.) Figure 4 confirms the absence of cross-flow coupling in the unbuckled range and gives an

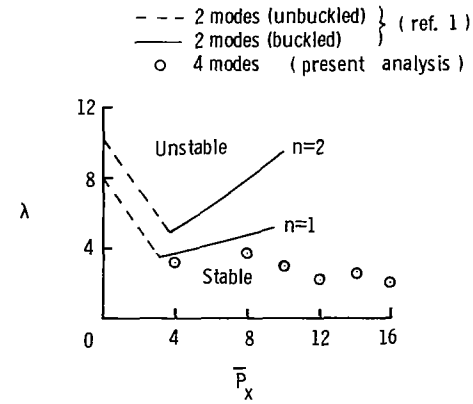

(a) $\nu = 1/2$.

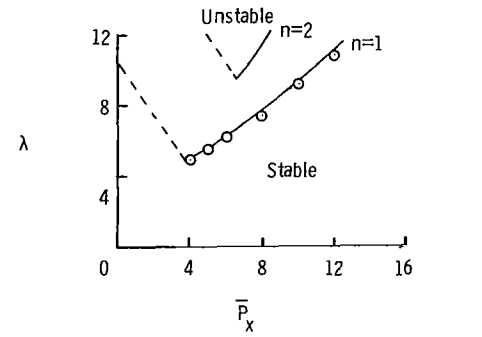

(b) $\nu = 1$.

Figure 5.- Flutter boundaries for panels with equal streamwise and cross-flow compressive loads. $\bar{P}_x = \bar{P}_y$.

indication of the validity of the procedure used in determining the flutter criterion. On the portion of the flutter boundary for buckled panels, cross-flow coupling of the modes has an effect on the flutter boundary for certain values of a/b and in-plane loading conditions. For the two square panels under streamwise loading and under biaxial loading (figs. 3(b) and 5(b)) the effects are negligible. However, for the panels shown in figures 3(a), 4, and 5(a), effects of cross-flow coupling on the flutter boundary are significant. For these cases (except for a region of fig. 3(a)), the effect of cross-flow coupling is to lower the flutter boundaries.

The results show that the effects of cross-flow coupling can be important in determining flutter boundaries for buckled panels. In this analysis no investigation is made of the convergence of the Galerkin solution. To do this more modes would have to be considered. In order to facilitate such a study, the modal solution that includes all the static buckling modes is presented in the appendix.

CONCLUDING REMARKS

A supersonic flutter analysis is presented for simply supported, rectangular panels subjected to specified in-plane compressive edge loads. A Galerkin procedure that utilizes the doubly infinite set of the static buckling modes yields a doubly infinite set of differential equations that can be reduced to any desired finite number of equations. The equations have been programed on an analog computer for a stability analysis for a four-mode solution that exhibits both streamwise and cross-flow coupling of the modes. The character of the output of the analog computer is then used to determine the critical flutter condition. Numerical results are presented for panels with ratios of length in the streamwise direction to length in the cross-flow direction equal to 1/2 and 1. The following specified in-plane boundary edge conditions are considered: (a) streamwise compressive loading only, (b) cross-flow compressive loading only, and (c) equal streamwise and cross-flow compressive loading. The results show that the effects of cross-flow coupling are important in determining flutter boundaries for buckled panels since the flutter speed can be appreciably reduced from the value determined without cross-flow coupling.

Langley Research Center,
National Aeronautics and Space Administration,
Langley Station, Hampton, Va., July 6, 1967,
126-14-02-24-23.

APPENDIX

ANALYSIS

The nonlinear differential equations expressing the equilibrium of an aerodynamically loaded oscillating panel based on Von Karman large-deflection plate theory are obtained in nondimensional form in reference 1. These equations can be written as follows:

$$\bar{u}_{,\xi\xi} + \frac{1-\mu}{2}\bar{u}_{,\eta\eta} + \frac{1+\mu}{2}\frac{b}{a}\bar{v}_{,\xi\eta} = -\frac{1}{2\pi^2}\left(\bar{w}_{,\xi}^{\,2} + \mu\bar{w}_{,\eta}^{\,2}\right)_{,\xi} - \frac{1}{\pi^2}\frac{1-\mu}{2}\left(\bar{w}_{,\xi}\bar{w}_{,\eta}\right)_{,\eta} \tag{1}$$

$$\frac{b}{a}\bar{v}_{,\eta\eta} + \frac{1-\mu}{2}\frac{b}{a}\bar{v}_{,\xi\xi} + \frac{1+\mu}{2}\bar{u}_{,\xi\eta} = -\frac{1}{2\pi^2}\left(\bar{w}_{,\eta}^{\,2} + \mu\bar{w}_{,\xi}^{\,2}\right)_{,\eta} - \frac{1}{\pi^2}\frac{1-\mu}{2}\left(\bar{w}_{,\xi}\bar{w}_{,\eta}\right)_{,\xi} \tag{2}$$

$$\frac{1}{\pi^4}\left(\bar{w}_{,\xi\xi\xi\xi} + 2\bar{w}_{,\xi\xi\epsilon\epsilon} + \bar{w}_{,\eta\eta\eta\eta}\right) - \frac{1}{\pi^2}\left(\bar{N}_x\bar{w}_{,\xi\xi} + \bar{N}_y\bar{w}_{,\eta\eta} + 2\bar{N}_{xy}\bar{w}_{,\xi\eta}\right) + \frac{3}{8}\lambda\bar{w}_{,\xi} + \bar{w}_{,\tau\tau} = 0 \tag{3}$$

where

$$\left.\begin{aligned}
\bar{N}_x &= \frac{1}{1-\mu^2}\left[\bar{u}_{,\xi} + \mu\frac{b}{a}\bar{v}_{,\eta} + \frac{1}{2\pi^2}\left(\bar{w}_{,\xi}^{\,2} + \mu\bar{w}_{,\eta}^{\,2}\right)\right] \\
\bar{N}_y &= \frac{1}{1-\mu^2}\left[\frac{b}{a}\bar{v}_{,\eta} + \mu\bar{u}_{,\xi} + \frac{1}{2\pi^2}\left(\bar{w}_{,\eta}^{\,2} + \mu\bar{w}_{,\xi}^{\,2}\right)\right] \\
\bar{N}_{xy} &= \frac{1}{2(1+\mu)}\left(\bar{u}_{,\eta} + \frac{b}{a}\bar{v}_{,\xi} + \frac{1}{\pi^2}\bar{w}_{,\xi}\bar{w}_{,\eta}\right)
\end{aligned}\right\} \tag{4}$$

in which $\bar{u}$, $\bar{v}$, and $\bar{w}$ are nondimensional displacements, $\bar{N}_x$, $\bar{N}_y$, and $\bar{N}_{xy}$ are nondimensional stress resultants, ξ and η are nondimensional x and y coordinates, τ is nondimensional time, μ is Poisson's ratio, and λ is the speed parameter.

The boundary conditions to be satisfied by $\bar{w}$ are the simple-support conditions

$$\left.\begin{aligned}
&\bar{w}(0,\eta,\tau) = \bar{w}(1,\eta,\tau) = \bar{w}(\xi,0,\tau) = \bar{w}\left(\xi,\frac{b}{a},\tau\right) = 0 \\
&\bar{w}_{,\xi\xi}(0,\eta,\tau) = \bar{w}_{,\xi\xi}(1,\eta,\tau) = \bar{w}_{,\eta\eta}(\xi,0,\tau) = \bar{w}_{,\eta\eta}\left(\xi,\frac{b}{a},\tau\right) = 0
\end{aligned}\right\} \tag{5}$$

The boundary conditions to be satisfied by $\bar{u}$ and $\bar{v}$ are those for uniform displacement of each edge in the plane of the plate

$$\bar{u}_{,\eta}(0,\eta,\tau) = \bar{u}_{,\eta}(1,\eta,\tau) = \bar{v}_{,\xi}(\xi,0,\tau) = \bar{v}_{,\xi}\left(\xi,\frac{b}{a},\tau\right) = 0 \tag{6}$$

and those for zero in-plane shear stress at the edge of the plate

$$\bar{v}_{,\xi}(0,\eta,\tau) = \bar{v}_{,\xi}(1,\eta,\tau) = \bar{u}_{,\eta}(\xi,0,\tau) = \bar{u}_{,\eta}\left(\xi,\frac{b}{a},\tau\right) = 0 \tag{7}$$

Appropriate boundary conditions for the edge loads are

$$\left.\begin{aligned} \frac{a}{b}\int_0^{b/a}\left(\bar{N}_x\right)_{\xi=0} d\eta = \frac{a}{b}\int_0^{b/a}\left(\bar{N}_x\right)_{\xi=1} d\eta = -\bar{P}_x \\ \int_0^1\left(\bar{N}_y\right)_{\eta=0} d\xi = \int_0^1\left(\bar{N}_y\right)_{\eta=\frac{b}{a}} d\xi = -\bar{P}_y \end{aligned}\right\} \tag{8}$$

and $\bar{P}_x$ and $\bar{P}_y$ are nondimensional in-plane edge loads per unit length.

The boundary conditions (eqs. (5), (6), and (7)) can be satisfied if the displacements $\bar{u}$ and $\bar{v}$ are written as

$$\left.\begin{aligned} \bar{u} = A_0 + A_1\xi + \sum_{m=1}^{\infty}\sum_{n=0}^{\infty} A_{mn} \sin m\pi\xi \cos\frac{n\pi a\eta}{b} \\ \bar{v} = B_0 + B_1\eta + \sum_{m=0}^{\infty}\sum_{n=1}^{\infty} B_{mn} \cos m\pi\xi \sin\frac{n\pi a\eta}{b} \end{aligned}\right\} \tag{9}$$

and if the normal displacement $\bar{w}$ is written as

$$\bar{w} = \sum_{m=1}^{\infty}\sum_{n=1}^{\infty} C_{mn} \sin m\pi\xi \sin\frac{n\pi a\eta}{b} \tag{10}$$

The nonlinear terms on the right-hand side of equations (1) and (2) can also be expanded in Fourier series as follows:

$$\left.\begin{aligned} \frac{1}{2\pi^2}\bar{w}_{,\xi}{}^2 = \sum_{m=0}^{\infty}\sum_{n=0}^{\infty} F_{mn} \cos m\pi\xi \cos\frac{n\pi a\eta}{b} \\ \frac{1}{2\pi^2}\bar{w}_{,\eta}{}^2 = \sum_{m=0}^{\infty}\sum_{n=0}^{\infty} G_{mn} \cos m\pi\xi \cos\frac{n\pi a\eta}{b} \\ \frac{1}{\pi^2}\bar{w}_{,\xi}\bar{w}_{,\eta} = \sum_{m=1}^{\infty}\sum_{n=1}^{\infty} H_{mn} \sin m\pi\xi \sin\frac{n\pi a\eta}{b} \end{aligned}\right\} \tag{11}$$

where

$$\left.\begin{aligned} F_{mn} &= \frac{2a}{b\pi^2\left(1+\delta_{m0}\right)\left(1+\delta_{0n}\right)}\int_0^{b/a}\int_0^1 \bar{w}_{,\xi}{}^2 \cos m\pi\xi \cos\frac{n\pi a\eta}{b}\,d\xi\,d\eta \\ G_{mn} &= \frac{2a}{b\pi^2\left(1+\delta_{m0}\right)\left(1+\delta_{n0}\right)}\int_0^{b/a}\int_0^1 \bar{w}_{,\eta}{}^2 \cos m\pi\xi \cos\frac{n\pi a\eta}{b}\,d\xi\,d\eta \\ H_{mn} &= \frac{4a}{b\pi^2}\int_0^{b/a}\int_0^1 \bar{w}_{,\xi}\bar{w}_{,\eta} \sin m\pi\xi \sin\frac{n\pi a\eta}{b}\,d\xi\,d\eta \end{aligned}\right\} \tag{12}$$

where

$$\delta_{mn} = 0 \qquad (m \neq n)$$

$$\delta_{mn} = 1 \qquad (m = n)$$

When equations (9) and (11) are substituted into equations (1) and (2) the coefficients A_{mn} and B_{mn} can be determined in terms of F_{mn}, G_{mn}, and H_{mn} as follows:

$$\left.\begin{aligned} A_{mn} &= -\frac{1}{\left[m^2+\left(\frac{na}{b}\right)^2\right]^2}\frac{1}{\pi}\left\{m\left[m^2+(2+\mu)\left(\frac{na}{b}\right)^2\right]F_{mn}+\left[\mu m^2-\left(\frac{na}{b}\right)^2\right]\left[mG_{mn}+\left(\frac{na}{b}\right)H_{mn}\right]\right\} \\ &\qquad (m = 1, 2, 3, \ldots, \infty;\ n = 0, 1, 2, \ldots, \infty) \\ B_{mn} &= -\frac{1}{\left[m^2+\left(\frac{na}{b}\right)^2\right]^2}\frac{a}{b\pi}\left\{\frac{na}{b}\left[(2+\mu)m^2+\left(\frac{na}{b}\right)^2\right]G_{mn}+\left[\mu\left(\frac{na}{b}\right)^2-m^2\right]\left[\left(\frac{na}{b}\right)F_{mn}+mH_{mn}\right]\right\} \\ &\qquad (m = 0, 1, 2, \ldots, \infty;\ n = 1, 2, 3, \ldots, \infty) \end{aligned}\right\} \tag{13}$$

The displacements $\bar{u}$ and $\bar{v}$ are now known in terms of A_0, A_1, B_0, B_1, F_{mn}, G_{mn}, and H_{mn}. The stress resultants are obtained in terms of the coefficients A_1, B_1, F_{mn}, G_{mn}, and H_{mn} by substitution from equations (9), (11), and (13) into equation (4). In order for $\bar{N}_x$ and $\bar{N}_y$ to satisfy the boundary conditions (eq. (8)), the constants A_1 and B_1 must have the values

$$\left.\begin{aligned} A_1 &= -\bar{P}_x + \mu\bar{P}_y - F_{00} \\ B_1 &= \frac{a}{b}\left(-\bar{P}_y + \mu\bar{P}_x - G_{00}\right) \end{aligned}\right\} \tag{14}$$

APPENDIX

where, when use is made of equations (10) and (12),

$$\left.\begin{aligned} F_{00} &= \frac{1}{8}\sum_{p=1}^{\infty}\sum_{q=1}^{\infty} p^2 C_{pq}{}^2 \\ G_{00} &= \frac{1}{8}\frac{a^2}{b^2}\sum_{p=1}^{\infty}\sum_{q=1}^{\infty} q^2 C_{pq}{}^2 \end{aligned}\right\} \tag{15}$$

The stress resultants become

$$\left.\begin{aligned} \bar{N}_x &= -\bar{P}_x + \sum_{n=1}^{\infty} F_{0n}\cos\frac{n\pi a\eta}{b} + \sum_{m=1}^{\infty}\sum_{n=1}^{\infty}\frac{\left(\frac{na}{b}\right)^2 J_{mn}}{\left[m^2+\left(\frac{na}{b}\right)^2\right]^2}\cos m\pi\xi\cos\frac{n\pi a\eta}{b} \\ \bar{N}_y &= -\bar{P}_y + \sum_{m=1}^{\infty} G_{m0}\cos m\pi\xi + \sum_{m=1}^{\infty}\sum_{n=1}^{\infty}\frac{m^2 J_{mn}}{\left[m^2+\left(\frac{na}{b}\right)^2\right]^2}\cos m\pi\xi\cos\frac{n\pi a\eta}{b} \\ \bar{N}_{xy} &= \sum_{m=1}^{\infty}\sum_{n=1}^{\infty}\frac{m\left(\frac{na}{b}\right)J_{mn}}{\left[m^2+\left(\frac{na}{b}\right)^2\right]^2}\sin m\pi\xi\sin\frac{n\pi a\eta}{b} \end{aligned}\right\} \tag{16}$$

where

$$J_{mn} = \left(\frac{na}{b}\right)^2 F_{mn} + m^2 G_{mn} + m\left(\frac{na}{b}\right)H_{mn} \tag{17}$$

When use is made of equations (12) and (14), F_{0n}, G_{m0}, and J_{mn} become

$$\left.\begin{aligned} F_{0n} &= \frac{1}{8}\sum_{p=1}^{\infty}\sum_{q=1}^{\infty}\sum_{s=1}^{\infty} p^2 C_{pq}C_{ps}\left[2\delta_{(s-q)n} - \delta_{(q+s)n}\right] && (n = 1, 2, \ldots, \infty) \\ G_{m0} &= \frac{1}{8}\frac{a^2}{b^2}\sum_{p=1}^{\infty}\sum_{r=1}^{\infty}\sum_{q=1}^{\infty} q^2 C_{pq}C_{rq}\left[2\delta_{(r-p)m} - \delta_{(p+r)m}\right] && (m = 1, 2, \ldots, \infty) \\ J_{mn} &= \frac{1}{8}\frac{a^2}{b^2}\sum_{p=1}^{\infty}\sum_{r=1}^{\infty}\sum_{q=1}^{\infty}\sum_{s=1}^{\infty} C_{pq}C_{rs}\Big\{2(mq+np)(ms+nr)\delta_{(r-p)m}\delta_{(q-s)n} + (mq-np)(ms-nr)\Big[2\delta_{(r-p)m}\delta_{(s-q)n} \\ &\quad - \delta_{(p+r)m}\delta_{(q+s)n}\Big] + 2(mq+np)(ms-nr)\Big[\delta_{(r-p)m}\delta_{(q+s)n} - \delta_{(p+r)m}\delta_{(s-q)n}\Big]\Big\} \end{aligned}\right\} \tag{18}$$

APPENDIX

Substitution of equations (10) and (16) into equation (3) and application of the Galerkin procedure yields

$$\frac{d^2C_{mn}}{d\tau^2} + \left\{\left[m^2 + \left(\frac{na}{b}\right)^2\right]^2 - m^2\bar{P}_x - \left(\frac{na}{b}\right)^2\bar{P}_y\right\}C_{mn} + \frac{3\lambda}{4}\sum_{p=1}^{\infty}\frac{pmC_{pn}}{\left(m^2 - p^2\right)}\left[1 - (-1)^{m+p}\right]$$

$$+ \frac{m^2}{2}\sum_{s=1}^{\infty}\sum_{q=1}^{\infty}C_{ms}F_{0q}\left[\delta_{(s+q)n} + \delta_{(s-q)n} - \delta_{(q-s)n}\right] + \frac{1}{2}\left(\frac{na}{b}\right)^2\sum_{r=1}^{\infty}\sum_{p=1}^{\infty}C_{rn}G_{p0}\left[\delta_{(r+p)m} + \delta_{(r-p)m} - \delta_{(p-r)m}\right]$$

$$+ \frac{1}{4}\frac{a^2}{b^2}\sum_{r=1}^{\infty}\sum_{p=1}^{\infty}\sum_{s=1}^{\infty}\sum_{q=1}^{\infty}\frac{(rq - sp)^2C_{rs}J_{pq}}{\left[p^2 + \left(\frac{qa}{b}\right)^2\right]^2}\left[\delta_{(r+p)m}\delta_{(s+q)n} + \delta_{(r-p)m}\delta_{(s-q)n} - \delta_{(r-p)m}\delta_{(q-s)n}\right.$$

$$\left. - \delta_{(p-r)m}\delta_{(s-q)n} + \delta_{(p-r)m}\delta_{(q-s)n}\right] + \frac{1}{4}\frac{a^2}{b^2}\sum_{r=1}^{\infty}\sum_{p=1}^{\infty}\sum_{s=1}^{\infty}\sum_{q=1}^{\infty}\frac{(rq + sp)^2C_{rs}J_{pq}}{\left[p^2 + \left(\frac{qa}{b}\right)^2\right]^2}\left[\delta_{(r+p)m}\delta_{(s-q)n}\right.$$

$$\left. - \delta_{(r+p)m}\delta_{(q-s)n} + \delta_{(r-p)m}\delta_{(s+q)n} - \delta_{(p-r)m}\delta_{(s+q)n}\right] = 0 \qquad (19)$$

The modal solution (eq. (19)) that utilizes the doubly infinite set of static mode shapes reduces to any desired approximate solution that uses a finite number of modes simply by deleting the undesired modes. In the present analysis numerical results are found for a four-mode solution so that

$$\bar{w} = \left(C_{11}\sin\pi\xi + C_{21}\sin 2\pi\xi\right)\sin\frac{\pi a\eta}{b} + \left(C_{12}\sin\pi\xi + C_{22}\sin 2\pi\xi\right)\sin\frac{2\pi a\eta}{b} \qquad (20)$$

and equation (19) becomes

$$\left.\begin{aligned}
&\ddot{C}_{11} + C_{11}\left(-M_1 + PC_{11}^2 + QC_{21}^2 + SC_{12}^2 + TC_{22}^2\right) + C_{21}\left(HC_{12}C_{22} - \lambda\right) = 0\\
&\ddot{C}_{21} + C_{21}\left(-M_2 + QC_{11}^2 + PC_{21}^2 + JC_{12}^2 + KC_{22}^2\right) + C_{11}\left(HC_{12}C_{22} + \lambda\right) = 0\\
&\ddot{C}_{12} + C_{12}\left(-M_3 + SC_{11}^2 + JC_{21}^2 + PC_{12}^2 + NC_{22}^2\right) + C_{22}\left(HC_{11}C_{21} - \lambda\right) = 0\\
&\ddot{C}_{22} + C_{22}\left(-M_4 + TC_{11}^2 + KC_{21}^2 + NC_{12}^2 + PC_{22}^2\right) + C_{12}\left(HC_{11}C_{21} + \lambda\right) = 0
\end{aligned}\right\} \qquad (21)$$

where

$$M_1 = \bar{P}_x + \nu^2\bar{P}_y - \left(1 + \nu^2\right)^2$$

$$M_2 = 4\bar{P}_x + \nu^2\bar{P}_y - \left(4 + \nu^2\right)^2$$

APPENDIX

$$M_3 = \bar{P}_x + 4\nu^2\bar{P}_y - (1 + 4\nu^2)^2$$

$$M_4 = 4\bar{P}_x + 4\nu^2\bar{P}_y - 16(1 + \nu^2)^2$$

$$P_1 = \frac{1}{16}(1 + \nu^4)$$

$$P_2 = \frac{1}{16}(16 + \nu^4)$$

$$P_3 = \frac{1}{16}(1 + 16\nu^4)$$

$$P_4 = 1 + \nu^4$$

$$Q = \frac{1}{16}\left[4(1 + \nu^4) + \frac{81\nu^4}{(1 + 4\nu^2)^2} + \frac{\nu^4}{(9 + 4\nu^2)^2}\right]$$

$$S = \frac{1}{16}\left[4(1 + \nu^4) + \frac{81\nu^4}{(4 + \nu^2)^2} + \frac{\nu^4}{(4 + 9\nu^2)^2}\right]$$

$$T = 16\left[\frac{\nu^4}{(1 + 9\nu^2)^2} + \frac{\nu^4}{(9 + \nu^2)^2}\right]$$

$$J = \frac{1}{16}\left[\frac{625\nu^4}{(1 + 9\nu^2)^2} + \frac{625\nu^4}{(9 + \nu^2)^2} + \frac{82\nu^4}{(1 + \nu^2)^2}\right]$$

$$K = \left[\frac{1}{4}(16 + \nu^4) + \frac{81\nu^4}{(16 + \nu^2)^2} + \frac{\nu^4}{(16 + 9\nu^2)^2}\right]$$

$$N = \left[\frac{1}{4}(1 + 16\nu^4) + \frac{81\nu^4}{(1 + 16\nu^2)^2} + \frac{\nu^4}{(9 + 16\nu^2)^2}\right]$$

$$H = 1 + \nu^4 + \frac{25\nu^4}{(1 + 9\nu^2)^2} + \frac{25\nu^4}{(9 + \nu^2)^2}$$

in which $\nu = a/b$. In equation (21) the double dots over the coefficients C_{mn} represent the second derivative with respect to τ. Equations (21) are set up on an analog computer in order to determine the flutter speed $\lambda = \lambda_{cr}$ as a function of the in-plane edge loads and a/b.

REFERENCES

1. Fralich, Robert W.: Postbuckling Effects on the Flutter of Simply Supported Rectangular Panels at Supersonic Speeds. NASA TN D-1615, 1963.

2. Kobayashi, Shigeo: Flutter of Simply Supported Rectangular Panels in a Supersonic Flow. Trans. Japan Soc. Aeron. Space Sci., vol. 5, no. 8, 1962, pp. 79-89.

3. Kobayashi, Shigeo: Two-Dimensional Panel Flutter. Trans. Japan Soc. Aeron. Space Sci., vol. 5, no. 8, 1962.
   I. Simply Supported Panel, pp. 90-102.
   II. Clamped Panel, pp. 103-118.

4. Dixon, Sidney C.: Experimental Investigation at Mach Number 3.0 of Effects of Thermal Stress and Buckling on Flutter Characteristics of Flat Single-Bay Panels of Length-Width Ratio 0.96. NASA TN D-1485, 1962.

5. Dowell, Earl H.: Nonlinear Oscillations of a Fluttering Plate. AIAA Paper No. 66-79, Jan. 1966.

6. Shideler, John L.; Dixon, Sidney C.; and Shore, Charles P.: Flutter at Mach 3 of Thermally Stressed Panels and Comparison With Theory for Panels With Edge Rotational Restraint. NASA TN D-3498, 1966.

7. Erickson, Larry L.: Supersonic Flutter of Flat Rectangular Orthotropic Panels Elastically Restrained Against Edge Rotation. NASA TN D-3500, 1966.

8. Dixon, Sidney C.: Comparison of Panel Flutter Results From Approximate Aerodynamic Theory With Results From Exact Inviscid Theory and Experiment. NASA TN D-3649, 1966.

9. Dugundji, John: Theoretical Considerations of Panel Flutter at High Supersonic Mach Numbers. AIAA J., vol. 4, no. 7, July 1966, pp. 1257-1266.

10. Ketter, D. J.: Flutter of Flat, Rectangular, Orthotropic Panels. AIAA J., vol. 5, no. 1, Jan. 1967, pp. 116-124.

NASA-Langley, 1968 —— 32 L-5040